Mapping of Milky Way Galactic Warp Using H1 Emissions

Max Lee *
Lab Partners: Basil Kyriacou, Connor McWard , James Mang

Department of Astronomy, University of California, Berkeley

Abstract

We use the $21\,cm$ neutral hydrogen line to develop a map of the Milky Way's warp through observations with a $4.7\,m$ radio telescope from galactic latitudes of $l = 0°$ to $l = 360°$ and longitudes of $b = -20°$ to $b = 20°$. We compare hydrogen clouds from above and below the plane and find evidence of contrasting emission profiles. Through our observations we estimate brightness temperatures contain a $\sim 66 \pm 5\%$ contribution from hydrogen clouds above the plane, and similarly, $72 \pm 5\%$ of gas cloud mass are in regions above the plane. These fractions come from limited regions in l, b providing strong evidence of a warped shape to the galaxy.

1 Introduction

Observing the Milky Way's structure is a formidable challenge. This is because describing the shape and features from the inside of it requires deep understanding of the physics that govern galactic dynamics. The discovery of neutral hydrogen's hyper-fine transition line (H1 from here on) has provided a breadth of insight into galactic structure because its energy corresponds to a predictable emission at $21\,cm$, which exists anywhere that an abundance of neutral hydrogen does.

Much of the Milky Ways disk consist of neutral hydrogen and instruments sensitive to the $21\,cm$ range have allowed progress in the field of galactic topography to expand. In this work we focus our attention to the asymmetry of hydrogen clouds above and below the galactic plane and provide evidence that a large scale warp exists. Work in this field was summarized in detail with Levine et al. [2006a], where $21\,cm$ topography was performed and the explicit Fourier modes of the warp and density profiles were mapped. Other works by Matsunaga [2012], have performed similar work but used cephids as tracers for this warping effect, while Schönrich and Dehnen [2018] has most recently used *GAIA*[Lindegren et al., 2018] photometric data of stars to further map it.

In this work we use observations of $21\,cm$ emissions to develop a mapping of neutral hydrogen near the galactic plane, and provide strong evidence that there exists an asymmetry in clouds both above and below it. We further perform an analysis of our mappings to find a fractional difference in temperature as well as mass above and below the plane.

The order of this work is as follows: In section 2 we discuss our instrumentation methods including our observational setup, data capturing procedures and temperature calibration. We then explain our methods of data analysis in section 3 and provide an in depth description of our steps towards developing two different maps of the galactic warp. We then discuss the quantitative features of the warp in section 4 and derive quantities describing it. We then conclude with some notes on errors in our process and areas we wish to improve upon for future work in section 5.

2 Instrumentation

In this work we use the *Leuschner Telsecope*, a $4.7\,m$ single dish radio telescope with beam width of $\sim 2.5°$. The *Leuschner Telsecope* is equipped with a spectrometer capturing 8192 frequency bins over a $12\,MHz$ range with an integration time of $\sim .69\,s$. We operate in the range of $144-156\,MHz$ by mixing our data with a Local Oscillator at $1270\,MHz$ to convert the $1420.406\,MHz$ hyper-fine line into a readable range for the dish.

The beam width of *Leuschner* is $\sim 2.5°$ so we sample the galaxy in $2°$ increments for a finer resolution of the hydrogen clouds and more detailed analysis. In total we capture 2389 10 second integration's of the milky way from $l = [0°, 360°]$ and $b = [-20°, 20°]$. Though we ideally would like to capture each one of the pointings, our northern latitude location makes this impossible.

Figure 1 shows true telescope pointings in right ascension (α) and declination (δ), where each pointing contains 10 seconds of integration. Our system temperature is $T_{sys} \sim 50\,K$, and because we are looking near the galactic plane in neutral hydrogen rich areas with temperatures at $T_{src} \sim 120\,K$, using the radiometer equation, we expect

our signal to noise ratio (SNR) to be,

$$\frac{S}{N} = \frac{T_{src}}{T_{sys}}\sqrt{\tau \Delta \nu} \tag{1}$$

Where τ is the integration time and $\Delta\nu$ is the bandwidth of the *Leuschner Telescopes* spectrometer at $\sim 1500\,Hz$. For each of our pointings, after averaging over our ~ 14 spectra, our SNR is ~ 10, which we believe is sufficient to begin analyzing our data.

2.1 Calibration

We calibrate the brightness temperature of the data $T_b(\nu)$ by taking measurements of the cold sky with a noise diode both turned on and off. We use,

$$G = \frac{T_{noise} - T_{cold}}{\sum(s_{noise} - s_{cold})} \sum s_{cold} \tag{2}$$

to find the gain; where T_{cold} is the temperature of the cold sky, $T_{cold} \sim 0, T_{noise}$ is the known value of the temperature diode, $\sim 80\,K$, and s_{noise}, s_{cold} are the spectra obtained. We find the gain to be $G = 30612.52$. As a check, we point towards Casseiopea A at $l = 120, b = 0$ (see fig 2) and find that the calibrated brightness temperature is $T_b \sim 120\,K$ which is what we would expect based off of previous observations (see BOYX collaboration "HI Observation near galactic anti-center"). Therefore, we continue with this value of the gain

We find that there is frequency dependant interference in our observations, which varies with pointings. We mitigate this through a fitting routine, where we first Fourier filter the lowest modes of the data, followed by a 12th degree polynomial fit of the off data values. This process is displayed in fig 2, which shows each step of the process and the final result.

From fig 2 we see that while our method is effective in reducing a majority of the band-pass signal and normalizing our data, there are discrepancies introduced. We find that for some of the smaller clouds of hydrogen, they are completely removed from this fitting routine (left two plots fig 2). Because we are interested in an overall warping effect of the galaxy, we believe that the errors introduced in our fitting do not effect our overall conclusion but add significantly to our uncertainty of measurements in section 3.

3 Analysis and Mappings

We compile all of our pointings and their respective fitted spectra into a voxel of shape $180 \times 20 \times 8192$, which represents all galactic latitudes, longitudes and frequency bins such that $T_b = T_b(l, b, \nu)$. For lines of sight that were unobtainable or that we missed, these values are set to

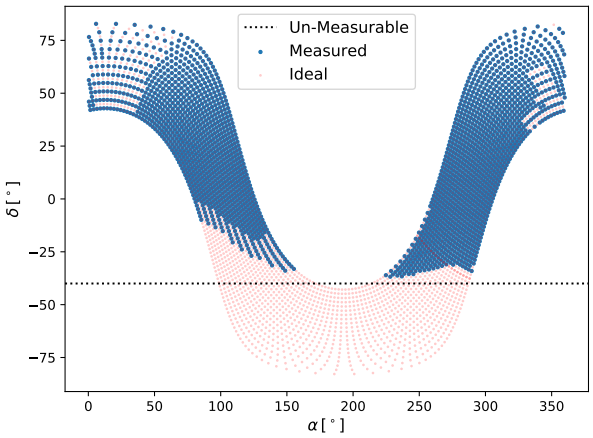

Figure 1: We show the multitude of our pointings, and highlight that any pointings below $\sim 40°\delta$ are unattainable due to our location in the northern hemisphere. We get a majority of samples from obtainable positionings in the alloted time that we had and the result is 2389 spectra in $2^c irc$ increments.

0. Similarly for all pointings that we don't symmetrically have above and below the plane, we exclude so that we are truly matching regions equally both above and below the plane. Our task is then to establish a way of expressing the three dimensional cube of data in a way that shows the galactic warp and which can be statistically analyzed to extrapolate quantitative information for description.

We do this in two ways, beginning with a simple mapping in frequency and galactic longitude space to test if there are differences in brightness temperatures above and below the galactic plane. We then convert our data into a galactocentric Cartesian frame, $T_b(l, b, \nu) - > T_b(x, y, z, \nu)$ and build a contour mapping of the galactic warp highlighting the mass difference in hydrogen clouds. We then use this in section 4 to consider the quantitative differences between the mappings that we present here.

3.1 Frequency and Longitude Mappings

Comparison between brightness temperatures above and below the galactic plane provides a direct relation to column density, N, or the number of hydrogen particles integrated along our line of sight through the relation,

$$N_{H1}(\nu) = 1.8 \times 10^{18} T_B(\nu) \Delta\nu \; cm^{-2} \tag{3}$$

Where v represents the velocity of the clouds, which we calculate using,

$$V_{doppler}(\nu) = c\frac{(\nu_0 - \nu)}{\nu_0} \tag{4}$$

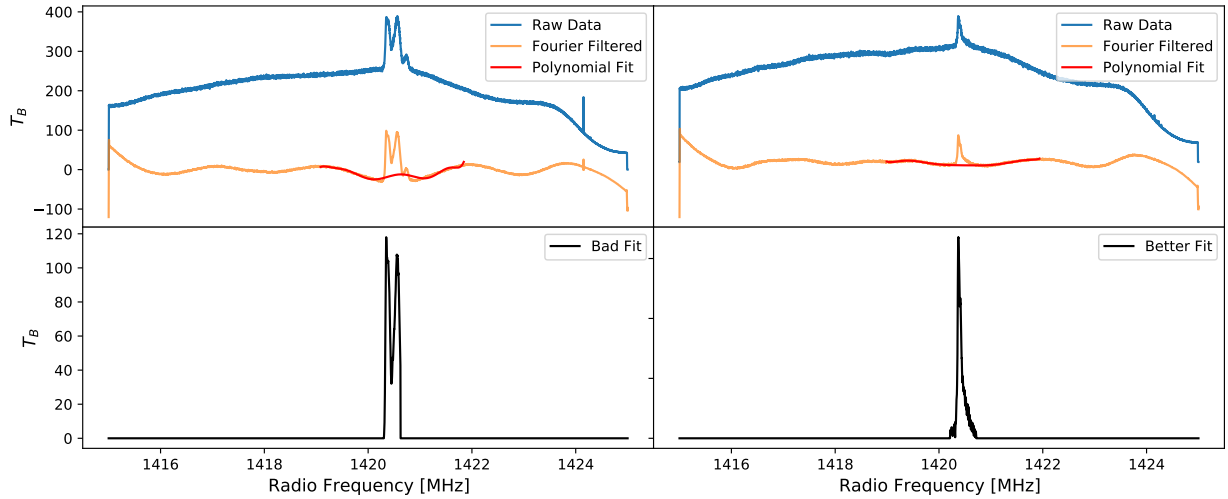

Figure 2: To calibrate the bandpass we use a two step cleaning routine where we first fourier filter the lowest modes of the data (*orange lines*), followed by a $12th$ degree polynomial fitting of the data around but not on the hydrogen signal (*red line*). We note the bounds of the polynomial fitting and subtract it off, zeroing all data points outside of the bounds. The result is the *black lines* in the bottom where we see that for some small features in the clouds as in the left plot, the fitting corrupts the data, removing small contributions completely, while for the majority of the data as seen in the left plot, we accurately calibrate out the filter. The left plot here is from $l = 120, b = 0$, and the right plot is $l = 18, b = 0$.

Here, c is the speed of light ν is a frequency in the spectra and ν_0 is the emission frequency of H1 at $1420.406\,MHz$.

Equation 3 gives us the hint that $N(\nu) \propto T_B(l, b, \nu)$, and therefore, calculating a temperature contrast above and below the plane provides a number density contrast. Areas where we don't find perfect symmetry in emissions correspond to asymmetries in column density.

We first use our voxel of data to present the galactic warp by performing an integrated average along the galactic latitude axis above and below the plane,

$$\langle T_{b,below}(l,\nu)\rangle_i = \frac{1}{b_{0,below}} \int_{b_{0,below}}^{0} T_b(l,b,\nu_i)db \quad (5)$$

Where $\langle\rangle_i$ denote average over the i^{th} frequency bin, $b_{0,below}$ is the lowest galactic latitude measurements below the plane, $b = -20°$ and s_i is the i^{th} frequency bin of the spectra. Equation 5 generalizes to above the galactic plane, but the bounds of the integral change to $0 \rightarrow b_{f,above}$ where the subscript f denotes the final latitude that we measure at ($b = 20°$).

Using these two spectra we can compute the temperature contrast that we define as,

$$T_{c,i}(l) = \langle T_{b,above}(l,\nu)\rangle_i - \langle T_{b,below}(l,\nu)\rangle_i. \quad (6)$$

If the milky way were perfectly symmetric, we would expect that this contrast was ~ 0 for all i bins, implying an equal amount of H1 emission and thus clouds above and below the galactic plane. We show in figure 6 that this is not the case, and in fact there appears to be portions in l that are dominated by emission from above the plane and others that are below the plane.

Of note in figure 6, are the regions between $15° \rightarrow 120°$ and $160° \rightarrow 220°$. in these regions we see that there are "hot spots" where the contrast in emission is extreme. We believe that these are indicative of the warping feature in the Milky Way. But to further probe it, we must account also for the distance to these sources.

3.2 Velocity Mapping

Our next goal is to convert our temperature observations into mass, but to do so requires knowledge of the distance to points in our spectra. This is obtainable by converting our spectra $T_b(l, b, \nu)$ into galactic Cartesian coordinates $T_b(x, y, z, v)$ where

$$\begin{aligned} l &= \arctan\left(\frac{x - x_\odot}{y - y_\odot}\right) \\ b &= \tan\left(\frac{z - z_\odot}{\sqrt{(x - x_\odot)^2 + (y - y_\odot)^2}}\right) \\ V_{radial} &= \left(\frac{V_\odot}{R} - \frac{V_\odot}{R_\odot}\right) R_\odot \sin(l)\cos(b) \end{aligned} \quad (7)$$

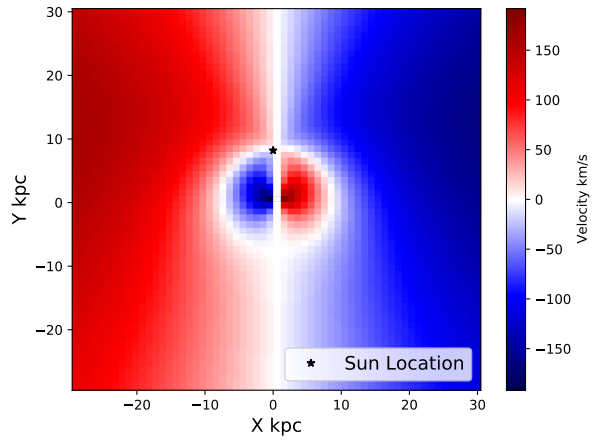

Figure 3: We interpolate our data onto a doppler velocity grid in galactocentric cartesian coordinates. To do this we determine the doppler velocity of each X and Y coordinate and match our spectra at the given l and b. Here we show the grid that we wish to match our data too.

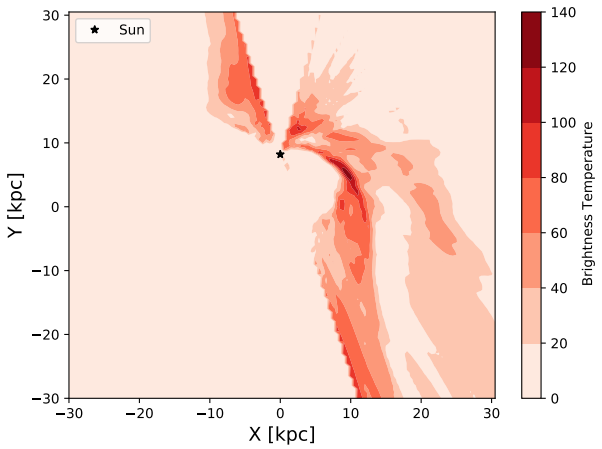

Figure 4: We interpolate the galactic plane to the velocity grid as seen in figure 3, and plot contours of the brightness temperatures. We can start to make out spiral arm structures, wrapping around the plane. We limit our interpolation to regions outside the solar circle, and away from 180° and 360° as suggested in Levine et al. [2006a]

In this transformation, x, y, z are the galctocentric coordinates in kpc, $x_\odot, y_\odot, z_\odot$ are the solar coordinates which we take to be $(0, 8.2\,kpc, 0)$, we assume a constant rotation curve such that all points have $V_\odot = 220\,km\,s^{-1}$ as motivated by Brand and Blitz [1993], and $R_\odot, R$ are the magnitudes of the x, y, z coordinates for the sun and Cartesian point respectively.

We interpolate our spectra into this frame by calculating the l, b angles for a given Cartesian position and using a linear interpolation to convert them to one for which we took data. We then find the corresponding velocity and temperature in our spectra using equation 4, matching it with the radial velocity in equation 7. Extracting the power corresponding to that velocity in the spectrum, and assigning the power to the correct position gives us the desired interpolation.

Because our sampling of the sky was every 2°, we use a linear interpolation such that the power assigned to each pixel is an average of the power at that location from four neighboring files. For example, at $l_{initial} = .5, b_{initial} = .5$, we use the files corresponding to $l = 0, 2$ and $b = 0, 2$ which are weighted with $|1 - (l_{initial}/2)\ mod\ 2|$ and $(l_{initial}/2)\ mod\ 2$, likewise for $b_{initial}$. Using this interpolation method, we are able to account for some of the discrepant data that we get from our fitting routine and more smoothly map our data.

Figure 3 shows the expected velocities for points in our grid given the position and motion of the sun and a flat rotation curve. We generate a grid that ranges from $-30 \rightarrow 30\,kpc$ in x and y and z with a pixel resolution of $0.5\,kpc$[3]. As suggested in Levine et al. [2006a], sources near 180° and 360° can be problematic in that velocities are too small when compared to their random velocities making distance estimates unreliable. We therefore exclude these regions from our mapping.

Figure 4 shows the result of the interpolation for the galactic plane where we see contours representing the brightness temperatures of our observations, placed into the galactocentric Cartesian coordinates. This is a good check on our interpolation progress, as we can compare the spiral structure of the Milky Way to known topographical maps. For example, we see that a long arcing arm starting at $\sim (10, 0)$, and spiraling just above the sun, which we take to be the Perseus arm as seen in similar contour plots, in Levine et al. [2006b]. In general we find that our contours generally match up with those seen in plot 1 of Levine et al. [2006b], giving us good reason to continue confidently with our analysis.

An advantage to our interpolated grid is that we can easily find the distance to points from our observing location by vector subtraction. This allows us to calculate the mass in the line of sight for each pointing,

$$M_{H1}(v) = 1.18 \times 10^{18} \Delta v d^2 m_h T_B(v) \Omega_b\ grams \quad (8)$$

Where Δv is the resolution of our velocity bins, Ω_b is the solid angle subtended by the beam, which is $(2.5°)^2$, m_h is the mass of a hydrogen atom, and d is the distance from the sun to the point on the grid. Using this we generate a contour map where levels represent the difference in mass above and below the galactic plane (fig 7).

While we see that there is a gradient implying an over density above and below the plane, we must exhibit caution and consider some sources of error in these calculations.

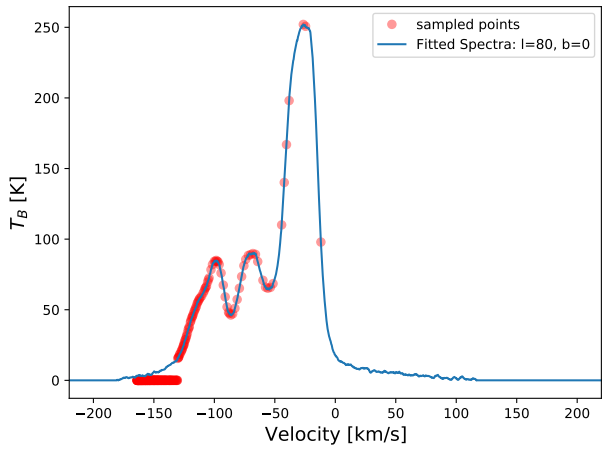

Figure 5: Interpolating our observations into a cartesian grid requires sampling our spectra at velocities that match with the expected velocitys using eq 4. But we find that through this process, not all of the spectra is sampled equally, leaving regions with significant velocity unaccounted for and others, over sampled. While most of the spectrum is salvaged during the interpolation, show one example of the sampling process at $l = 80°$, $b = 0$.

For starters, because our resolution of the grid was fairly low, our sampling of velocity was uneven. (see fig 5). This means our brightness temperatures used in mass calculations can underestimate masses in many locations while in some lines of sight, assign many more values from region of the spectra. We see these in the contour plots such as fig 7, as streaks moving radially outward from the sun location and in fig 5 as the densely sampled region in the far negative velocities. Because of our generic and even interpretation of the velocity curve of the Milky Way, it could lead to this sampling issue. But, we suspect that because of this evenness the sampling error would happen at the same spectra above and below the galactic plane equally. So we believe that while our entire galactic plane may have inaccuracies with sampling, the difference in the mass's should be mostly a fair comparison.

4 Discussion

The temperature and mass contrasts that we find in section 3 provides strong evidence of galactic asymmetry. In this section we make this observation quantitative by finding the fractional difference in brightness temperature and mass from both of our maps to quantify the level of asymmetry that exists.

We must note that because of the fitting routine adding to power through out each spectra and the noted sampling problems as seen by the streaking effects in both figure 4 and figure 7, this value contains a significant amount of error. With the fitting routines removing small clouds on the 5% level (only small clouds that are $\sim$ 5% the contributions to spectra are removed from some files), we believe that assigning an error of 5% to all following calculations is fair.

We first calculate the percent of emission that we observe to be in access above the galactic plane. We do this by summing over all negative (or positive) differences in temperature and dividing by the total sum of temperature contributions. This ratio gives the the percentage of matter above and below. We find using this that $66.24 \pm 5\%$ of the emissions observed come from below the galactic plane while, the remaining come from above.

To test if our mappings coincide with one another, we also calculate the fractional mass difference using the same routine but for figure 7. Here we find that the Mass contrast is $72.6 \pm 5\%$ where above the plane we find $4.21 \times 10^{10} M_\odot$ difference and below the plane we find, $11.19 \times 10^{10} M_\odot$.

From this we find that not only do our graphs coincide with each other, but that through our assumptions, the mass of the warp is indeed tractable, and we are able to find quantitative values representing the level at which the warp exists.

5 Conclusion

In this work we observed the structure of the Milky Way galaxy's warp through observation of 21 cm neutral hydrogen emissions. We found that there is an over-density of hydrogen clouds in the upper latitudes of the milky way from $\sim 15 - 120°$ and that at $\sim 160°$ there begins to be a an over density in the lower latitudes. We used our observations and expected velocities to interpolate our data to a grid in galctocentric Cartesian coordinates and from this were able to further view the warp in terms of mass instead of brightness temperature.

We found that when observing the brightness temperature of the milky way there was a $\sim 66 \pm 5\%$ over density in the upper latitudes and similarly when comparing the mass above and below there was a $\sim 72 \pm 5\%$ difference. This provides strong evidence of a warped structure to the milky way galaxy.

Through this work. we discussed the main points where error into our data was introduced, and this also gives us an idea of future work to further mitigate it. We would like in the future to perform a similar analysis but with a higher resolution that allows for us to better sample, and with a more robust fitting mechanism that ensure the quality of data for each spectra is preserved. Further, because we are only able to observe the sky from the northern hemisphere, we would like to get more data from the south to fill in the gaps in our data and develop a 360° view of the warp.

6 Acknowledgements

We would like to thank Professor Parsons for his help in understanding, and analyzing the data, as well as for providing support and accomidations in this unprecedented time. For this work I completed most of the observations and data reduction. Connor James and Basil worked on the capturing script and we all worked together on deciding a direction to go with our analysis. Also we would like to thank Frank for his trips out Leuschner Telescope during a pandemic, thanks Frank.

References

E. S. Levine, Leo Blitz, and Carl Heiles. The vertical structure of the outer milky way HiDisk. *The Astrophysical Journal*, 643(2):881–896, jun 2006a. doi: 10.1086/503091. URL https://doi.org/10.1086%2F503091.

N. Matsunaga. Cepheids as Tracers of the Galactic Structure and Evolution. In W. Aoki, M. Ishigaki, T. Suda, T. Tsujimoto, and N. Arimoto, editors, *Galactic Archaeology: Near-Field Cosmology and the Formation of the Milky Way*, volume 458 of *Astronomical Society of the Pacific Conference Series*, page 231, August 2012.

Ralph Schönrich and Walter Dehnen. Warp, waves, and wrinkles in the Milky Way. , 478(3):3809–3824, August 2018. doi: 10.1093/mnras/sty1256.

L. Lindegren, J. Hernández, A. Bombrun, S. Klioner, U. Bastian, M. Ramos-Lerate, A. de Torres, H. Steidelmüller, C. Stephenson, D. Hobbs, U. Lammers, M. Biermann, R. Geyer, T. Hilger, D. Michalik, U. Stampa, P. J. McMillan, J. Castañeda, M. Clotet, G. Comoretto, M. Davidson, C. Fabricius, G. Gracia, N. C. Hambly, A. Hutton, A. Mora, J. Portell, F. van Leeuwen, U. Abbas, A. Abreu, M. Altmann, A. Andrei, E. Anglada, L. Balaguer-Núñez, C. Barache, U. Becciani, S. Bertone, L. Bianchi, S. Bouquillon, G. Bourda, T. Brüsemeister, B. Bucciarelli, D. Busonero, R. Buzzi, R. Cancelliere, T. Carlucci, P. Charlot, N. Cheek, M. Crosta, C. Crowley, J. de Bruijne, F. de Felice, R. Drimmel, P. Esquej, A. Fienga, E. Fraile, M. Gai, N. Garralda, J. J. González-Vidal, R. Guerra, M. Hauser, W. Hofmann, B. Holl, S. Jordan, M. G. Lattanzi, H. Lenhardt, S. Liao, E. Licata, T. Lister, W. Löffler, J. Marchant, J. M. Martin-Fleitas, R. Messineo, F. Mignard, R. Morbidelli, E. Poggio, A. Riva, N. Rowell, E. Salguero, M. Sarasso, E. Sciacca, H. Siddiqui, R. L. Smart, A. Spagna, I. Steele, F. Taris, J. Torra, A. van Elteren, W. van Reeven, and A. Vecchiato. Gaia Data Release 2. The astrometric solution. , 616:A2, August 2018. doi: 10.1051/0004-6361/201832727.

J. Brand and L. Blitz. The velocity field of the outer galaxy. , 275:67–90, August 1993.

E. S. Levine, Leo Blitz, and Carl Heiles. The spiral structure of the outer milky way in hydrogen. *Science*, 312(5781):1773–1777, 2006b. ISSN 0036-8075. doi: 10.1126/science.1128455. URL https://science.sciencemag.org/content/312/5781/1773.

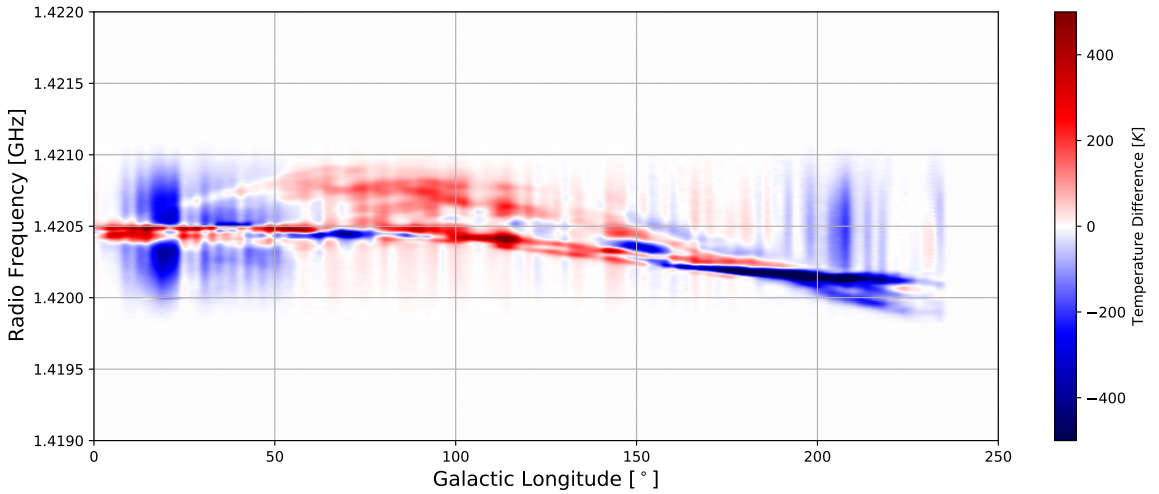

Figure 6: The galactic warp can be imaged by subtracting all emissions from above the galactic plane and subtracting it with the equivalent measurements from below. Here we present this difference as a function of frequency, with the *blue* regions representing areas that were over dense in the upper latitudes and the red regions representing the over densities in the lower latitudes. The darker the coloring the more of a contrast between the two are. We see here our first evidence that there exists a contrast in the matter placement outside of the galactic plane.

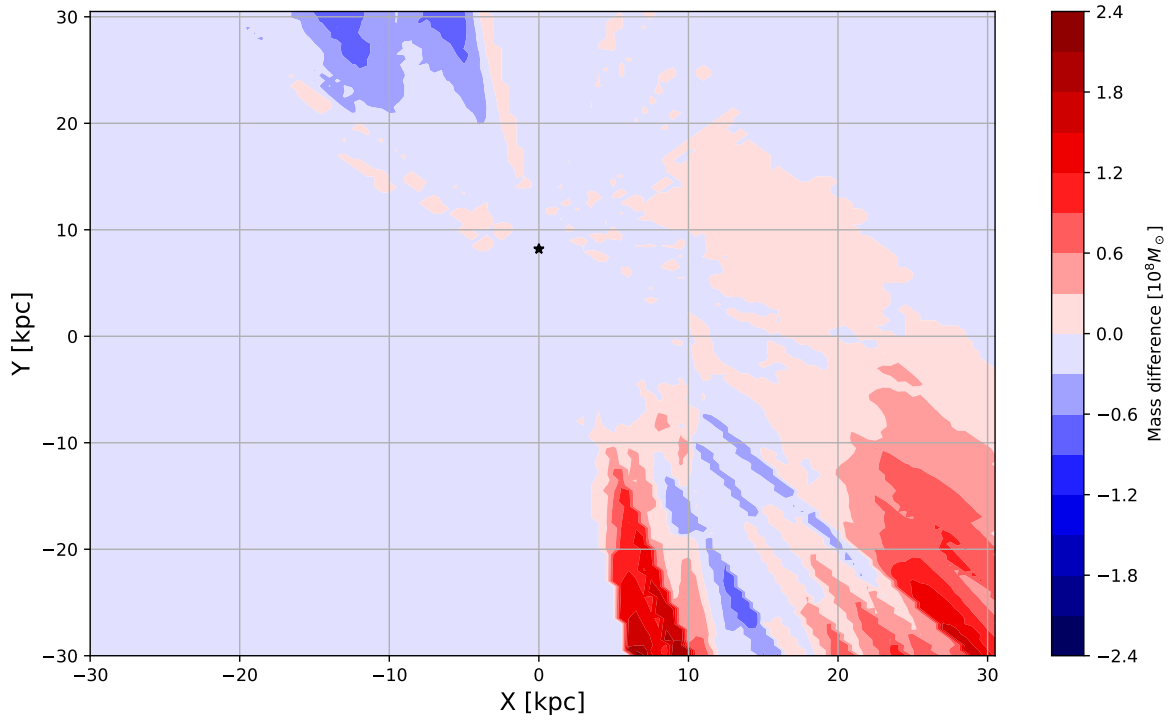

Figure 7: An interpolation of our spectra into galctocentric Cartesian coordinates allows us to calculate distances to sources. This lets us weigh the temperature measurements by distances and calculate actual mass quantities. We calculate the mass of our observations and sum them both above and below the plane. The difference between these two sums yields a mass contrast representative of the galactic warp. We find regions where above the plane dominates the mass (*Red contours*), and some regions where below dominates (*Blue contours*). Because we are limited to observations by our earth location, we do not get a full 360° image of the warp but we do start to see some symmetry in the location of the warps location.